

Final Draft
of the original manuscript:

Fu, T.; Li, W.Y.; Huetsch, L.; Hilgert, J.; Wang, F.F.; dos Santos, J.F.; Huber, N.:
**Effects of tool rotational and welding speed on microstructure
and mechanical properties of bobbin-tool friction-stir welded
Mg AZ31**

In: *Materials and Design* (2014) Elsevier

DOI: [10.1016/j.matdes.2014.07.023](https://doi.org/10.1016/j.matdes.2014.07.023)

**Effects of tool rotational and welding speed on microstructure and mechanical properties of
bobbin-tool friction-stir welded Mg AZ31**

T. Fu¹, W.Y. Li^{1*}, L. Hütsch², F.F. Wang¹, J.F. dos Santos², N. Huber³

¹ State Key Laboratory of Solidification Processing, Shaanxi Key Laboratory of Friction Welding Technologies, Northwestern Polytechnical University, Xi'an 710072, Shaanxi, PR China

² Helmholtz-Zentrum Geesthacht, Institute of Materials Research, Materials Mechanics, Solid-State Joining Processes (WMP), Geesthacht 21502, Germany

³ Helmholtz-Zentrum Geesthacht, Institute of Materials Research, Materials Mechanics, Geesthacht 21502, Germany

* Corresponding author: Wenya Li. Email: liwy@nwpu.edu.cn

Abstract

The effects of rotational and welding speeds on the microstructure and mechanical properties of bobbin-tool friction-stir welded (BT-FSW) Mg AZ31 were investigated. The results indicated that the thermo-mechanically affected zone (TMAZ) consisted of equiaxed grains, which were inconsistent with the deformed, rotated and elongated grains found in the TMAZs of BT-FSWed Al alloys and friction-stir welded Al and Mg alloys. The average grain size increased as the ratio of the rotational speed to welding speed increased. Excellent welds with no degradation in hardness were produced using a low heat input. Tensile tests revealed that the ultimate tensile strengths gradually increased with increasing welding speed while keeping the rotational speed constant while the rotational and welding speeds had only slight influences on the yield stresses and fracture elongations.

Keywords: Bobbin-tool friction-stir welding; AZ31 Mg alloy; Microstructure; Mechanical property

1. Introduction

Recently, the increasing demand to reduce fuel consumption and associated costs has led to the replacement of heavy components with lighter alloys in the automotive and aerospace industries. Mg alloys have become a lucrative option for replacing heavier components due to their low densities, high mechanical stiffnesses and environmental friendliness [1]. However, Mg alloys have a very strong

affinity for oxygen and other chemical oxidants and can readily oxidize in the weld zone during fusion welding [2]. Other problems associated with conventional fusion welding of Mg alloys are related to defects that form during solidification, such as porosity, hot cracking, and partial melting, which degrade the mechanical properties of the joint. Therefore, a reliable joining technique is required to support the implementation of Mg alloys in the transportation industry.

Friction-stir welding (FSW) is a solid-state joining technique which was invented by TWI Ltd. in 1991 [3]. This welding technique avoids problems related to solidification when welding Mg alloys because of the avoidance of bulk melting during the welding process. Residual stresses and associated distortion can be notably reduced because the welding temperatures are significantly lower compared to those used in conventional fusion welding techniques [2]. To date, FSW has been widely applied to join various Mg alloys, such as Mg-Al-Zn [4], Mg-Zn-Y [5] and Mg-Al-Ca alloys [6].

To enable welding of closed sections without the need of a backing bar, which is required in conventional FSW to accommodate the loads applied during welding, an alternative tool configuration has been proposed [3] named bobbin-tool friction-stir welding (BT-FSW), as shown in Fig. 1. This process configuration employs two rotating shoulders which are connected by a probe: upper (acting on the upper surface of the parent material) and lower (acting on the lower surface of the parent material) shoulders. Due to the presence of the lower shoulder, the process loads are confined within the tool.

To date, the available literature concerning BT-FSW is still considerably less compared to conventional FSW. Lally et al. [7] studied FSWed and BT-FSWed AA6056 joints and observed that the microstructures of the joints were identical for both welding techniques but that the tensile strength and elongation were slightly lower for the BT-FSW joints than for the FSWed joints. Wan et al. [8] reported that the weld shape of the BT-FSWed joint differed from that of the weld produced using conventional FSW and has been reported to be similar to an hourglass shape. Liu et al. [9] investigated BT-FSWed 6061-T6 joints and observed that the strengthening meta-stable precipitates diminished in the stir zone (SZ) and TMAZ. However, such efforts primarily focused on Al alloys; attempts to use BT-FSW for Mg alloys are rather limited, particularly regarding the effects of the processing parameters on the microstructure and properties of the joint. Therefore, this work aims to investigate the effects of the tool rotational speed (ω) and welding speed (v) on the microstructure and mechanical properties of the BT-FSWed joint in the Mg alloy AZ31.

2. Materials and experimental procedures

2.1. Materials and welding parameters

In the present study, 2-mm-thick rolled AZ31B-O Mg alloy sheets were used. The nominal chemical composition of the as-received material is presented in Table 1. The processing parameters used to produce the various joints are shown in Table 2. The ratio ($\delta=\omega^2/(v\times 10^4)$), shown in Table 2, is used in to discuss the effects of heat input on the microstructure and mechanical properties as δ is the main influential factor of the resulting temperature [10]. The welding direction was perpendicular to the rolling direction.

2.2 Analysis and testing

The specimens for metallographic examination were sectioned perpendicular to the welding direction. Polished samples were obtained using standard metallographic procedures and were etched with a reagent consisting of 100 ml of a 2 wt% oxalate solution and 2 ml of concentrated nitric acid to reveal the micro- and macrostructures. Microstructure analysis was performed using an optical microscope (OM: OLYMPUS GX51) and the Image-Pro Plus software was used to measure the grain size.

The microhardness profiles were obtained using a Vickers hardness tester (Duramin-A300) with a load of 0.2 kg and a dwell time of 10 s. The space between indentations was 0.25 mm along the mid-thickness of the weld region.

Tensile tests were performed on the as-welded specimens at room temperature using a screw-driven tensile testing machine. A testing speed of 0.2 mm/min and an extensometer base length of $L_0=50$ mm were used. The tensile properties of each joint were evaluated using three tensile specimens cut from the same joint.

3. Results and discussion

3.1 Microstructure analysis

Fig. 2 shows the microstructure of the parent material (PM). The PM exhibits a typical rolled structure with inhomogeneous equiaxed grains [11, 12]. The average grain size was determined to be 6.8 μm .

A typical macrograph of the cross-section of the BT-FSWed weld (sample D) is shown in Fig. 3. The SZ, TMAZ and heat-affected zone (HAZ) can be clearly identified in the joint. The shape of the SZ

differs from that found in BT-FSW Al alloys. Monica et al. [13] reported that a discernable pattern similar to “fingers” appeared in the central region of the SZ in BT-FSW 6061-T651. However, the SZ in this study is dumbbell shaped, as indicated by the dashed line in Fig. 3. Similar hourglass shapes of the SZ are observed in BT-FSWed AA6061-T6 [9] and AA6082-T6 [8].

High-magnification images of the three observed zones of Fig. 3 are presented in Fig. 4. The SZ consists of equiaxed grains, which can be attributed to the dynamic recrystallization (DRX) that resulted from the combination of frictional heating, intense plastic deformation and viscous dissipation due to the rotation of the tool during welding. Similar results have been reported in the literature [12, 14]. The grains in the upper and lower zones of all the SZs (Figs. 4b and 4c) are larger than those in the center zone of the SZ (Fig. 4a). The reason for the larger grains in these zones is that the temperature in the zones near the shoulders is higher. Padmanaban et al. [15] also found that the grains in the SZ near shoulders were coarser than other grains in FSWed AZ31B joints. Fig. 4(d) shows the grains in the TMAZ, which are primarily equiaxed grains. It should be noted, that such a phenomenon has not been observed in the TMAZs of BT-FSWed Al alloys and FSWed Al and Mg alloys. For BT-FSWed Al alloys [7, 8, 13], the grains in the TMAZ have been reported to be severely deformed, rotated and elongated due to plastic deformation caused by interaction with the tool, and these grains generally do not recrystallize. The equiaxed grains in the TMAZ indicate that recrystallization has in fact occurred. DRX occurs more easily in Mg alloys than in Al alloys [16] because of its low stacking fault energy, few slip systems and low recrystallization temperature [17]. Thus, the TMAZ has microstructural features similar to those of the SZ, and therefore, the boundary lines between the TMAZ and SZ are not as obvious as those in Al alloy joints. However, in the FSWed AZ61A joints investigated by Rajakumar et al. [18], elongated and deformed grains were observed in the TMAZ. These observations were explained by insufficient deformation strain and thermal exposure within this region. Compared to FSW, DRX during BT-FSW occurs more easily outside of the SZ due to the additional heat source represented by the second shoulder. In the HAZ (Fig. 4e), the microstructure appears similar to the PM. This result is consistent with a previous report [1].

Moreover, Fig. 5 clearly shows that the grains are smaller and more homogeneous in the TMAZ of the advancing side (AS) compared to that of the retreating side (RS). This observation is similar to the results obtained by Forcellese et al. [19] in FSWed AZ31B joints. The main reason for this result is that the relative speed in the AS is larger than that in the RS because the rotation and displacement are in

the same direction in the AS. Thus, the localized frictional heat could be greater in the AS, resulting in a fuller DRX and a faster nucleation rate [20].

Fig. 6 shows the microstructures in and near the flash for sample D. Coarse grains can be observed in these locations. These zones correspond to a larger shear force and higher heat input, which lead to the acceleration of grain growth.

The OM images of SZs at different δ are shown in Fig. 7. In addition, the average grain sizes of the SZs generated at different δ were measured and are plotted in Fig. 8a. It is clear that the average grain size increases with increasing δ , except for sample A ($\delta=1.93$).

The heat input during BT-FSW is crucial to the joint properties and is affected by welding conditions such as the rotational and welding speeds. Chang et al. [21] developed the following relations to calculate the peak temperature in the SZ:

$$\ln d = 9.0 - 0.27 \ln Z \quad (1)$$

$$T = \frac{Q}{R \left(\ln Z - \ln \frac{\omega \pi R_{SZ}}{H_{SZ}} \right)} \quad (2)$$

where d represents the grain size of the SZ, Z is the Zener-Hollomon parameter, ω is the tool rotational speed, Q is the activation energy for lattice diffusion (135 kJ/mol [22]), R is the gas constant, T is the absolute temperature in the SZ, and R_{SZ} and L_{SZ} are the average radius and depth of the SZ, respectively. In this study, R_{SZ} and L_{SZ} are estimated to be approximately 6 mm and 2 mm, respectively.

The SZ temperatures calculated using equations (1) and (2) at different δ are plotted in Fig. 8b. It is observed that the SZ temperature could be described by the ratio δ and that it increases with increasing δ .

A larger heat input during welding provides more energy for grain growth [4]. Furthermore, higher welding speeds will lead to higher strain rates [23], which in turn activate more strain-free nucleation sites [24]. The faster the nucleation rate is, the finer the grain size will become [24]. Hence, the grain size increases as δ increases. For the AZ31B Mg alloy used in this study, the grain growth or refinement corresponds to a critical δ (i.e., 2.5). Compared to the grain size in PM, the grains in the SZ will be coarsened if $\delta > 2.5$, but on the contrary, the grains will be refined if $\delta < 2.5$.

Notably, sample B ($\delta=2.45$) exhibits a tunnel defect in the SZ, as shown in Fig. 9. The voids are

generally found close to the TMAZ in FSW welds [25]. There are two mechanisms for the formation of voids [11]: (i) volume deficiency and (ii) inadequate material flow and mixing. The poor stirring or mixing may be caused by low heat input; however, the voids in this work were only observed in sample B ($\delta=2.45$), which does not correspond to the low heat input (Fig. 8b). Additionally, there is no obvious volume deficiency during welding. Therefore, further research may be necessary to determine the reasons for the void formation observed in this study.

3.2 Microhardness

Fig. 10 shows the microhardness profiles along the mid-thickness of the joints welded at different δ . It is observed that the PM exhibits hardness values of 60-65 HV. Compared to the PM, an increase in hardness of the SZ is clearly observed at low δ (e.g., 1.93 and 2.45), as shown in Fig. 10. At high δ (larger than 2.5), on the other hand, the hardnesses of all joints show little variation, and the hardness values fluctuate between 50 HV and 75 HV. The above results are similar to the observations in FSWed AZ31 [22] and AZ91D [26] joints.

The changes in hardness are mainly related to the grain size variation, dislocation density and distribution of small particles of intermetallic compounds [27, 28, 29]. The AZ31B used in this study is not a particle-strengthened material; thus, according to the Hall-Petch equation, grain refinement plays an important role in strengthening [22]. At low δ , the hardness in the SZ is larger than that in the PM due to the finer grains, which is consistent with many previously reported findings in the FSW of Mg alloys [18, 27, 25].

As indicated in Fig. 8a, the grain size in the SZ is larger than that in the PM when $\delta>2.5$. Hence according to the Hall-Petch relationship, the hardness in these SZs should be smaller than that in the PM, but the hardness values in the SZ and PM are almost identical. This result may be related to other strengthening factors, such as dislocation density and residual stress [22]. Esparza et al. [27] reported that there was a slight increase in hardness in the SZs of FSWed Al or Mg alloy joints in which no reprecipitation or related aging/annealing effects occurred due to the relatively high dislocation density. In FSW AZ31 welds [30], the hardness profiles also showed slight variation and fluctuation (50~60 HV) as the rotational speed increased from 800 to 3500 rpm.

The hardness values in the AS are slightly larger than those in the RS (Fig. 10). This result can be attributed to the finer grains in the AS than in the RS. This observation agrees with the findings in

FSWed AZ31 joints generated using a ‘pinless’ tool [19] and in FSWed Al-Mg-Sc alloy joints [31].

There are some differences in the microhardness profiles of the BT-FSWed joints in Al and Mg alloys. In BT-FSWed 6061-T651 welds, Monica [13] observed that the hardness values were inferior to those in the PM, exhibiting a “w”-shaped profile. This phenomenon has also been observed by other researchers in FSWed and BT-FSWed Al alloys [7, 32]. They stated that the changing profile shape is closely associated with the distribution of the precipitation phase because the Al alloys used are precipitation-hardened alloys. In this study, however, the intermetallic phases in AZ31 are small and AZ31 is not a particle-strengthened material.

3.3 Tensile properties

To investigate the strengths of the welds, tensile tests were conducted. The stress-strain curve of sample A is presented in Fig. 11. All of the tensile test results are summarized in Fig. 12. It is clearly observed from Fig. 12 that the ultimate tensile strengths (UTS) of all joints are lower than that of the PM. In addition, the yield stresses (YS) of almost all of the joints are approximately 90.0 MPa, which are significantly lower compared to the YS (268.0 MPa) of the PM. This result indicates that the rotational and welding speeds have only a slight impact on the YS of the joint. **The yield strength for Az31 should be in the regime between 150 and 180 MPa. Please check your data.**

With increasing welding speed, the UTS gradually increases when the rotational speed is held constant. However, with increasing rotational speed, the UTS remains almost constant when the welding speed is held constant (see Fig. 12b). As shown in Fig. 8b, a higher welding speed generates lower heat, leading to a smaller grain size of the BT-FSWed joints. Materials with a smaller grain size would impose more restrictions to dislocation movement and have a higher resistance to localized plastic deformation due to a greater number of grain boundaries [33, 34]. Therefore, the UTS gradually increases at higher welding speeds when the rotational speed is held constant, which is consistent with the finding in BT-FSW 6061 joints [9].

Sample I exhibits the highest YS (97.3 MPa) and UTS (231.9 MPa) but presents a relatively small fracture elongation (FE) of ~1.61%. The FEs of all joints are remarkably lower: approximately one-tenth of the FE of the PM. The above results demonstrate that the welding speeds remarkably impact the UTS of BT-FSWed AZ31 joints. The tensile properties of the BT-FSWed joints in this study are lower than those of FSWed AZ31 joints [30, 35, 36] because of the larger heat input caused by the

two shoulders. This phenomenon was also observed by Lally et al. [7] in FSWed and BT-FSWed joints in Al alloys, and they stated that the loss in UTS reaches 20% for BT-FSWed joints in Al alloys. Yang et al. reported that the joint efficiency of FSWed AZ31 joints could reach 95.2% [30], but the maximum joint efficiency is only 81% in this study. **Pleaes check your data once you have corrected for the right yield strength.**

4. Conclusions (what you have written is a summary of the results, not a conclusion)

(1) The TMAZ consists of equiaxed grains rather than the rotated and elongated grains present in the TMAZs of BT-FSWed Al alloys and FSWed Al and Mg alloys. The grains in the upper and lower zones of the SZ are coarser than those in the central zone of the SZ.

(2) Compared to the grain size in the PM, the grains in the SZ are coarsened if $\delta > 2.5$, but on the contrary, the grains are refined if $\delta < 2.5$. In addition, the hardness in the SZ is slightly greater than that in the PM when $\delta < 2.5$, but there are little variations in hardness throughout the joint when $\delta > 2.5$.

(3) The tensile test results demonstrate that the UTS gradually increases with increasing welding speed when the rotational speed is held constant, but the rotational and welding speeds have only a slight impact on the YS and FE of the joint. An excellent joint with the highest YS (97.3 MPa) and UTS (231.9 MPa) is obtained, but this joint exhibits an FE as low as 1.61%. **I am not certain if this needs to be said so explicitly within the conclusions.**

Acknowledgements

The work reported in this study has been conducted for the reference project “Crashworthiness of Magnesium Sheet Structures” (CraMaSS). This project has been conducted within the scope of activities of the Research Platform “Lightweight Materials Assessment, Computing and Engineering Centre” (ACE). ACE is a part of the Materials Mechanics Division in the Institute of Materials Research of the Helmholtz-Zentrum Geesthacht. The authors also would like to acknowledge financial support from the Fok Ying-Tong Education Foundation for Young Teachers in the Higher Education Institutions of China (131052), the Fundamental Research Fund of NPU and the 111 Project (B08040).

References

[1] T. Nagasawa, M. Otsuka, T. Yokota, T. Ueki, *Magnes. Technol.* 2000 (2000) 383-387.

- [2] A.R. Rose, K. Manisekar, V. Balasubramanian, *J. Mater. Eng. Perform.* 21 (2012) 257-265.
- [3] W.M. Thomas, E.D. Nicholas, J.C. Needham, M.G. Church, P. Templesmith, C.J. Dawes, International Patent, Application No. PCT/GB92, Patent Application No. 9,125,978.8, 1991.
- [4] W.B. Lee, Y.M. Yeon, S.B. Jung, *Mater. Sci. Technol.* 19 (2003) 785-790.
- [5] S. Mironov, Y. Motohashi, R. Kaibyshev, *Mater. Trans.* 48 (2007) 1387-1395.
- [6] D.T. Zhang, M. Suzuki, K. Maruyama, *Acta Metall. Sinica.* 19 (2006) 335-340.
- [7] A.L. Lally, D. Alléhaux, F. Marie, C. Daile Oonne, G. Biallas, *Weld. World.* 50 (2006) 98-106.
- [8] L. Wan, Y.X. Huang, Z.I. Lv, S.X. Lv, J.C. Feng, *Mater. Des.* 55 (2014) 197-203.
- [9] H.J. Liu, J.C. Hou, H. Guo, *Mater. Des.* 50 (2013) 872-878.
- [10] W.J. Arbegast, P.J. Hartley, *Proceedings of the Fifth International Conference on Trends in Welding Research (Eds.)*, Pine Mountain, GA, USA, 1998, 541.
- [11] X. Cao, M. Jahazi, *Mater. Des.* 30 (2009) 2033-2042.
- [12] N. Afrin, D.L. Chen, X. Cao, M. Jahazi, *Mater. Sci. Eng. A* 472 (2008) 179-186.
- [13] M. Torres, The University of Texas, 2011.
- [14] N. Afrin, D.L. Chen, X. Cao, M. Jahazi, *Scr. Mater.* 57 (2007) 1004-1007.
- [15] G.V. Padmanaban, S.J.K. Sundar, *J. Mater. Eng. Perform.* 19 (2010) 155-165.
- [16] S. H. C. Park, Y. S. Sato, H. Kokawa, *Script Mater.* 49 (2003) 161-166.
- [17] S.E. Ion, F.J. Humphreys, S.H. White, *Acta Metall.* 30 (1982) 1909-1919.
- [18] S. Rajakumar, V. Balasubramanian, A. Razalrose, *Mater. Des.* 49 (2013) 267-278.
- [19] A. Forcellese, F. Gabrielli, M. Simoncini, *Mater. Des.* 34 (2012) 219-229.
- [20] M. Fatmi, B. Ghebouli, M.A. Ghebouli, T. Chihi, M.A. Hafiz, *Physica B.* 406 (2011) 2277-2280.
- [21] C.I. Chang, X.H. Du, J.C. Huang, *Script Mater.* 59 (2008) 356-359.
- [22] L. Commin, M. Dumont, J.E. Masse, L. Barrallier, *Acta Mater.* 57 (2009) 326-334.
- [23] K.A.A Hassan, P.B. Prangnell, A.F. Norman, D.A. Price, S.W. Williams, *Sci. Technol. Weld.* 8 (2003) 257-268.
- [24] M. Pareek, A. Polar, F. Rumiche, J.E. Indacochea (Eds.), *Proceedings of the 7th International Conference on Trends in Welding research*, Callaway Gardens resort, Pine Mountain, Georgia, USA, 2005, 421-426.
- [25] X. Cao, M. Jahazi, *Mater. Des.* 32 (2011) 1-11.
- [26] H.C. Seung, A. Yutak, K. Hiroyuki, *J. Mater. Sci.* 38 (2003) 4379-4383.

- [27] J.A. Esparza, W.C. Davis, E.A. Trillo, *J. Mater. Sci. Lett.* 21 (2002) 917-920
- [28] A. Razal Rose, K. Manisekar, V. Balasubramanian, *Trans. Nonferrous Met. Soc. China* 21 (2011) 974-984.
- [29] L. Zhou, K. Nakata, J. Liao, *Mater. Des.* 42 (2012) 505-512.
- [30] J. Yang, D. Wang, B.L. Xiao, D.R. Ni, Z.Y. Ma, *Metall. Mater. Trans. A* 44 (2013) 517-530.
- [31] K. Subbaiah, M. Geetha, M. Govindaraju, *Trans. Indian Inst. Met.* 65 (2012) 155-158.
- [32] M. Skinner, R.L. Edwards, *Mater. Sci. Forum.* 426 (2003) 2849-2854.
- [33] H.C. Seung, A. Yutak, K. Hiroyuki, *J. Mater. Sci.* 38 (2003) 4379-4383.
- [34] S.H. Chowdhury, D.L. Chen, S.D. Bhole, X. Cao, P. Wanjara, *Metall. Mater. Trans. A* 44 (2013) 323-336.
- [35] R.D. Fu, H.S. Ji, Y.J. Li, L. Liu, *Sci. Technol. Weld.* 17 (2012) 174-179.
- [36] J. Yang, B.L. Xiao, D. Wang, Z.Y. Ma, *Mater. Sci. Eng. A* 527 (2010) 708-714.

Figure and Table captions

Table 1. Chemical composition (wt.%) of the AZ31B Mg alloy.

Table 2. Processing parameters for producing the BT-FSWed joints.

Fig. 1. Schematic of BT-FSW.

Fig. 2. Microstructure of the parent material.

Fig. 3. A typical macroscopic image of the BT-FSWed joint.

Fig. 4. Typical microscopy images of sample D: (a) central zone of the SZ, (b) upper layer of the SZ, (c) lower layer of the SZ, (d) TMAZ and (e) HAZ.

Fig. 5. Microstructure of TMAZ (a: at advancing side, b: at retreating side).

Fig. 6. Microstructures in (a) and near (b) the flash in sample D.

Fig. 7. Microstructures of the SZs at different values of δ : (a) 1.93, (b) 2.45, (c) 2.63, (d) 3.34, (e) 3.38 and (f) 4.59.

Fig. 8. Effects of δ on (a) grain size and (b) temperature in the SZ.

Fig. 9. Tunnel defect in the SZ of sample B.

Fig. 10. Hardness profiles along the mid-thickness of joints welded under different δ .

Fig. 11. Example stress-strain curves of sample A.

Fig. 12. Tensile test results for the PM and of all joints: (a) YS, (b) UTS and (C) FE

Table 1. Chemical composition (wt.%) of the AZ31B Mg alloy.

<i>Al</i>	<i>Zn</i>	<i>Mn</i>	<i>Si</i>	<i>Ni</i>	<i>Fe</i>	<i>Mg</i>
3.01	0.9	0.5	0.04	0.005	0.005	bal.

Table 2. Processing parameters for producing the BT-FSWed joints.

<i>No.</i>	ω (<i>rpm</i>)	v (<i>mm/min</i>)	δ
A	900	24	3.38
B	900	33	2.45
C	900	42	1.93
D	1050	24	4.59
E	1050	33	3.34
F	1050	42	2.63
G	1200	24	6.00
H	1200	33	4.36
I	1200	42	3.43

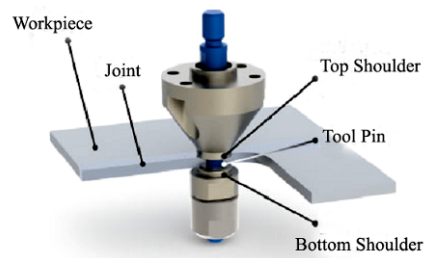


Fig. 1. Schematic of BT-FSW.

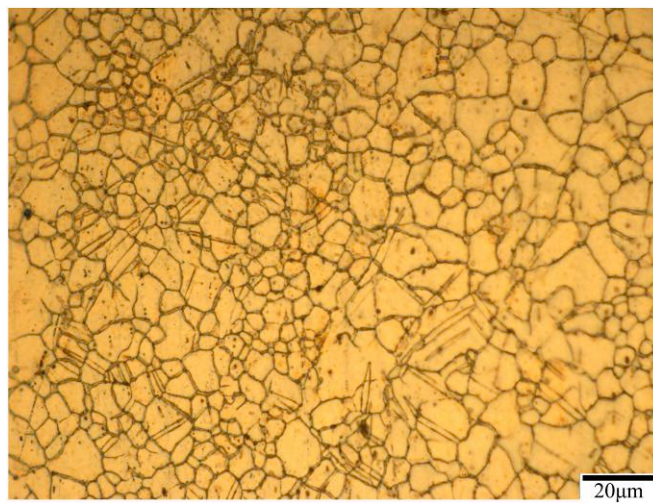


Fig. 2. Microstructure of the parent material.

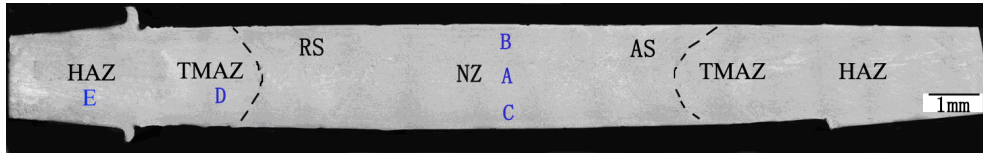


Fig. 3. A typical macroscopic image of BT-FSWed joint

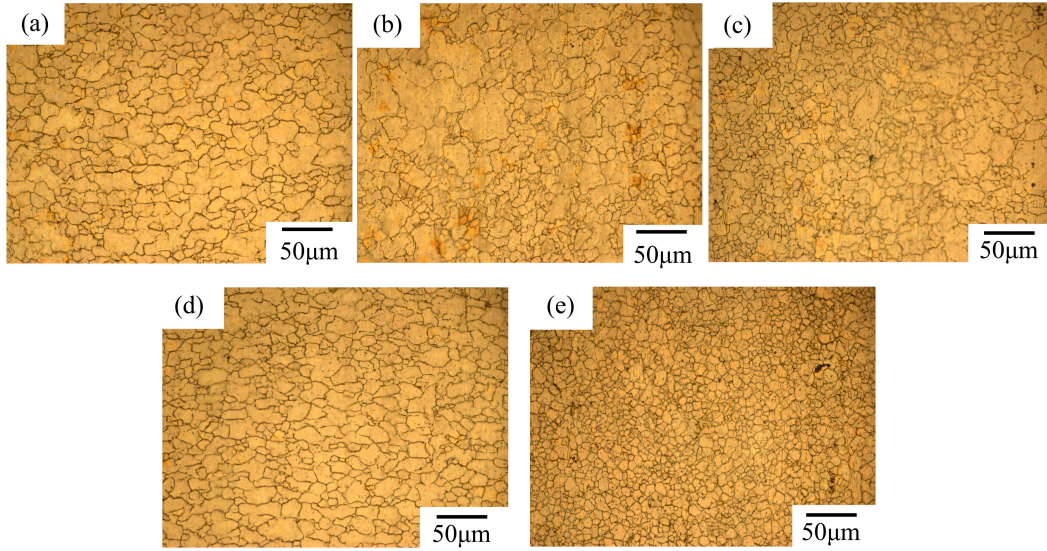


Fig. 4. Typical microscopy images of sample D: (a) central zone of the SZ, (b) upper layer of the SZ, (c) lower layer of the SZ, (d) TMAZ and (e) HAZ.

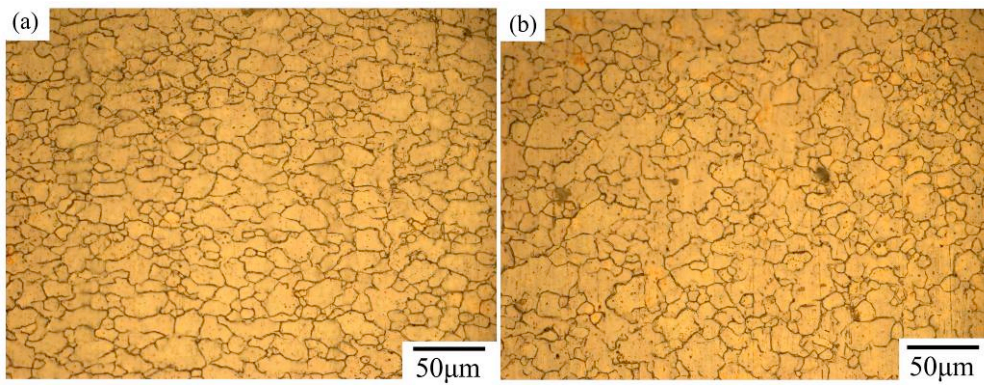
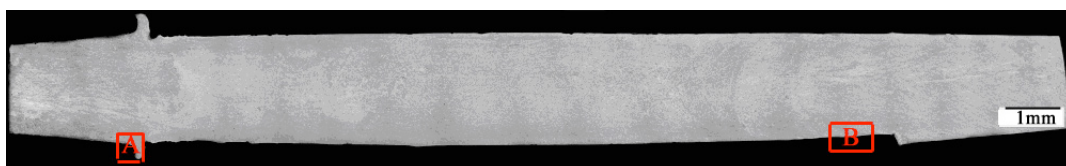


Fig. 5. Microstructure of TMAZ (a: at advancing side, b: at retreating side).



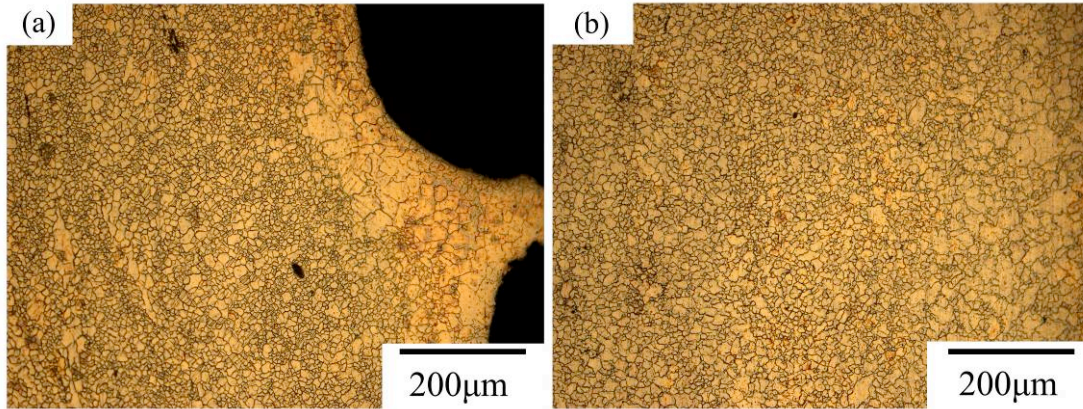


Fig. 6. Microstructures in (a) and near (b) the flash in sample D.

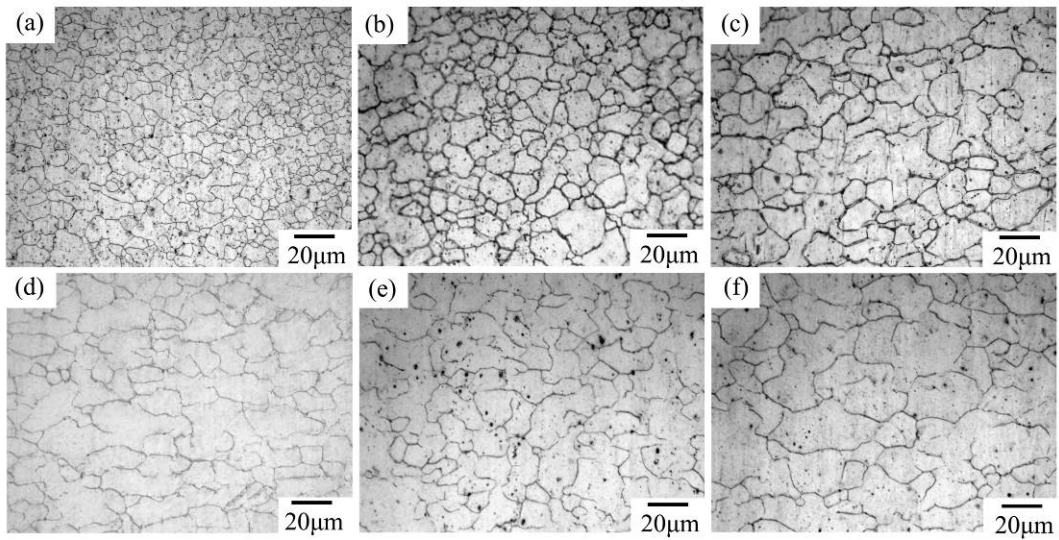


Fig. 7. Microstructures of the SZs at different values of δ : (a) 1.93, (b) 2.45, (c) 2.63, (d) 3.34, (e) 3.38 and (f) 4.59.

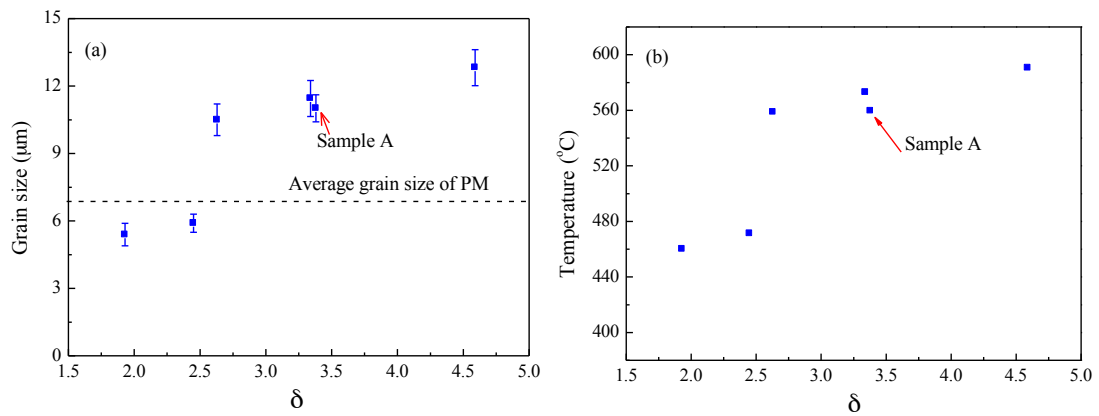


Fig. 8. Effects of δ on (a) grain size and (b) temperature in the SZ.

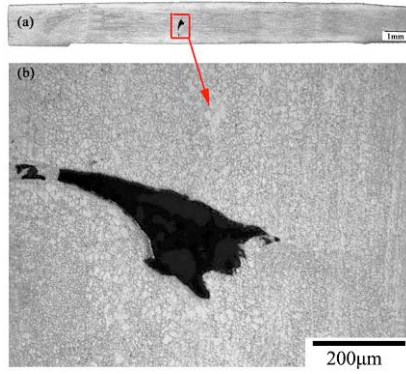


Fig. 9. Tunnel defect in the SZ of sample B.

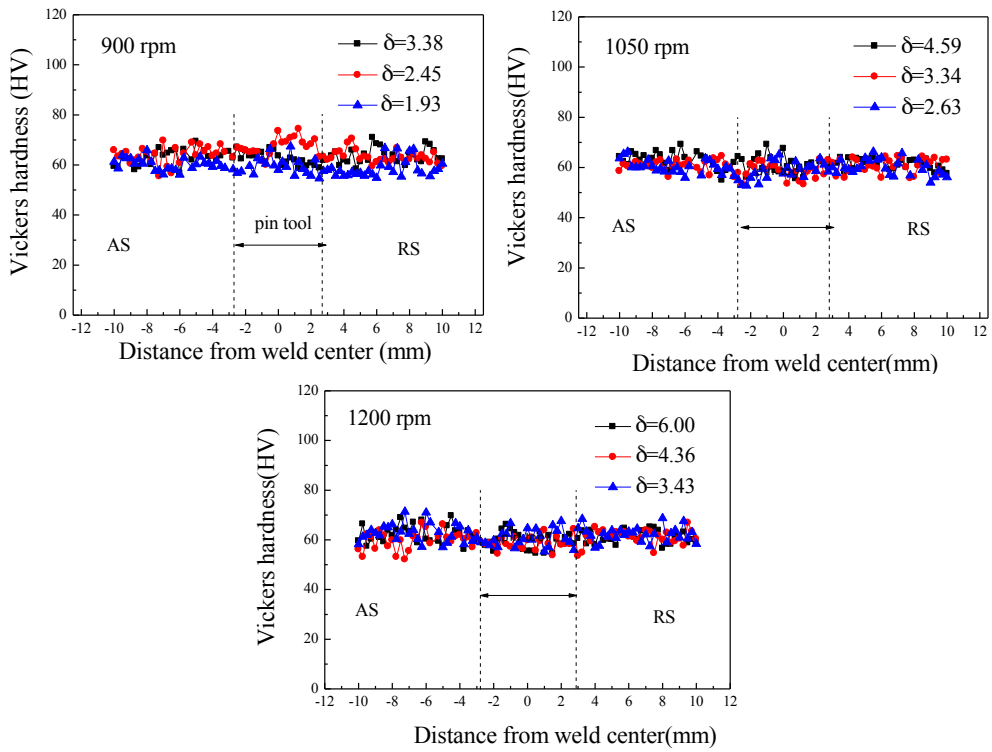


Fig. 10. Hardness profiles along the mid-thickness of joints welded under different δ .

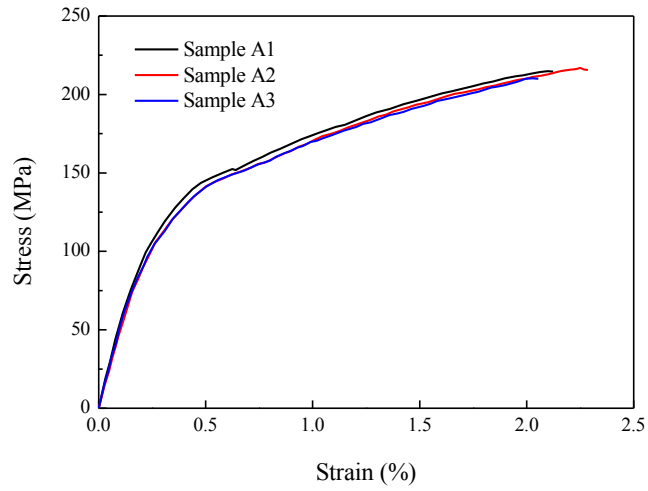


Fig. 11. Example stress-strain curves of sample A.

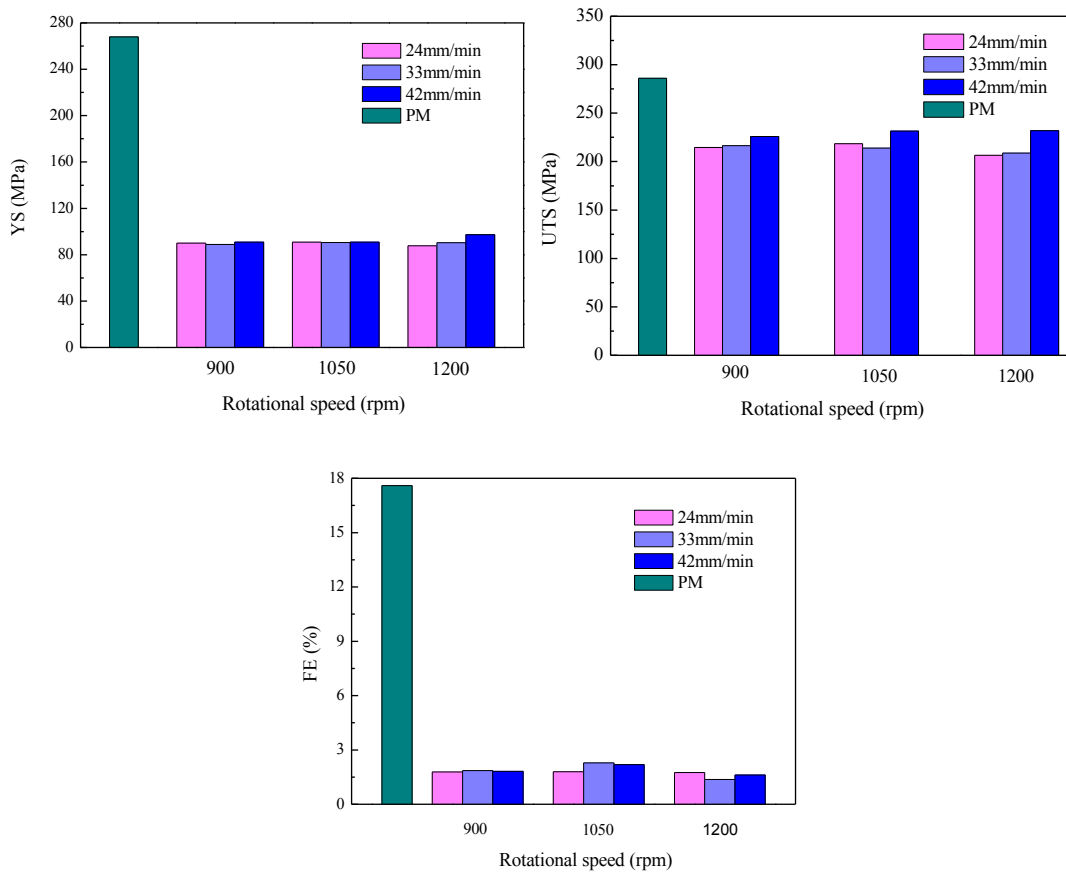


Fig. 12. Tensile results for the PM and of all joints: (a) YS, (b) UTS and (c) FE